Hindawi Publishing Corporation
Advances in Civil Engineering
Volume 2014, Article ID 745814, 11 pages
http://dx.doi.org/10.1155/2014/745814

Research Article

Free Vibration Response of a Frame Structural Model Controlled by a Nonlinear Active Mass Driver System

Ilaria Venanzi and Filippo Ubertini

Department of Civil and Environmental Engineering, University of Perugia, Via G. Duranti 93, 06025 Perugia, Italy

Correspondence should be addressed to Ilaria Venanzi; ilaria.venanzi@unipg.it

Received 21 November 2013; Revised 24 February 2014; Accepted 24 February 2014; Published 27 March 2014

Academic Editor: John Mander

Active control devices, such as active mass dampers, are mainly employed for the reduction of wind-induced vibrations in high-rise buildings, with the final aim of satisfying vibration serviceability limit state requirements and of meeting appropriate comfort criteria. When such active devices, normally operating under wind loads associated with short return periods, are subjected to seismic events, they can experience large amplitude vibrations and exceed stroke limits. This may lead to a reduced performance of the control system that can even worsen the performance of the whole structure. In this paper, a nonlinear control strategy based on a modified direct velocity feedback algorithm is proposed for handling stroke limits of an active mass driver (AMD) system. In particular, a suitable nonlinear braking term proportional to the relative AMD velocity is included in the control law in order to slowdown the device in the proximity of the stroke limits. Experimental and numerical free vibration tests are carried out on a scaled-down five-story frame structure equipped with an AMD to demonstrate the effectiveness of the proposed control strategy.

1. Introduction

Active control systems are in principle very effective for the mitigation of the structural response, especially for high-rise buildings and flexible structures that may experience significant wind-induced vibrations [1, 2]. However, their use in practical applications is still limited by the physical bounds of the devices. In the case of strong earthquakes, the limits of the actuators may be exceeded, forcing the system to operate in a nonlinear mode for which it was not designed, thus worsening the performance of the controlled structure. The physical bounds of the actuators include both the control force limits and the stroke limits.

The problem of force saturation has been deeply studied in the literature. Some approaches deal with preventing saturation of the control signal by designing the control system to always operate below its limits in the framework of linear control [3]. Another category of control methods accounts for system limitations directly in the control algorithm. Chase et˜al. [4] modified the H_{∞} control method through the addition of nonlinear state-dependent terms in order to model the actuators saturation and the uncertainties in the parameters of the system. Indrawan et al. [5] developed the bound-force control method which excludes the control-effort penalty from the performance index defined in the case of LQR control, defines it at the end of each time interval, and seeks the optimal control force for each time interval. Another control strategy based on solving in real time the classic linear quadratic regulator (LQR) problem with adaptive weights and system matrices is represented by the "state-dependent Riccati equation" (SDRE) [6, 7]. Materazzi and Ubertini [8] developed an application of the SDRE for fully constrained systems with both physical limits and actuators saturation. A state feedback control law and an observer-based controller were proposed by Kim and Jabbari [9]. The bang-bang control, which minimizes a performance index subjected to the control force constraint, has been widely investigated by several authors. The main shortcoming of the bang-bang control is the undesirable control chattering near the origin of the state space due to high frequency switching of the control force. To overcome this problem, Mongkol et al. [10] proposed the linear saturation (LS) control algorithm that consists of a low-gain linear controller when the system is close to the zero state and a bang-bang controller

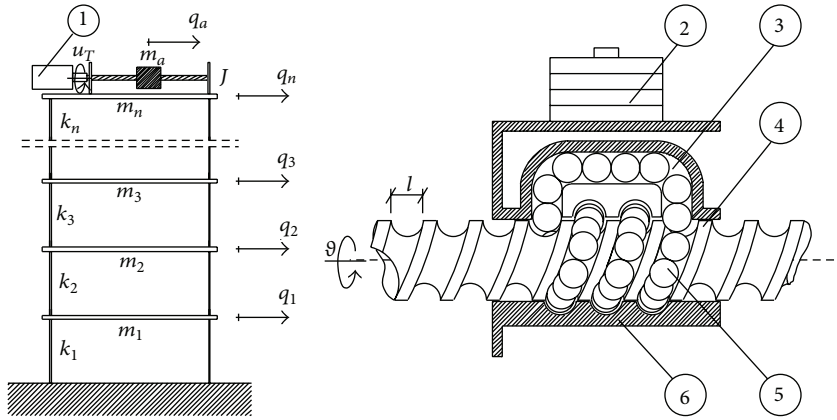

Figure 1: Multistory frame structure with AMD made of electric torsional servomotor (element 1) and ball screw (a); detailed view of ball screw components (b): additional carried mass (2), return tube (3), screw (4), bearing balls (5), and ball nut (6).

otherwise. Wu and Soong [11] introduced the suboptimal bang-bang control strategy described by a function of the state where the control force is determined by minimizing the time derivative of a quadratic Lyapunov function under the control force constraint. This method was found to be effective under a certain range of control force but it can be unstable outside of this range. To overcome this instability, Lim [12] proposed an adaptive bang-bang control algorithm.

The problem of exceeding the stroke limits is perhaps the most important constraint for application of AMD systems to actual structures, but it has not been widely discussed in the literature. Nagashima and Shinozaki [13] developed a variable gain feedback (VGF) control for buildings equipped with AMD systems. The variable feedback gain is a function of a quantity representing the tradeoff between the reduction of the building response and the amplitude of the mass stroke, and this quantity is on-line controlled to keep the stroke within its limits. Yamamoto and Sone [14] utilized a linearly variable gain proportional to an index representing the activity of an AMD, that is, a function of its stroke displacement, the first modal frequency of the controlled building, and the stroke limit of the AMD. Within the framework of the state-dependent Riccati equation, Friedland [7] proposed to apply to the system a physical constraint modeled by a nonlinear spring which provides a state-dependent restoring force that is accounted for in the controller design.

Authors have recently started a research program on innovative solutions for structural control. On one side, analytical studies on the definition of original control algorithms for constrained systems and on the optimization of noncollocated control systems [15, 16] were developed. On the other side, laboratorial experimental work has been carried out to implement a control system made of an active mass driver system [17]. The prototype AMD is made of a torsional electric servomotor that moves a small mass through a ball screw.

In this paper a nonlinear control strategy is proposed that is capable of preventing crossing of the stroke limits of an AMD system. To this aim, a skyhook control algorithm is modified by adding to the control force a nonlinear term that increases in the vicinity of the stroke bounds. To reduce the impulsive effect of this additional braking term, the function smoothly varies within the fixed boundaries. To demonstrate the effectiveness of the proposed approach, experimental tests were carried out on a reduced-scale five-story frame structure equipped with the AMD and subjected to free vibration tests. The effect of a variation in the parameters defining the nonlinear control force is discussed and the optimal choice of such parameters is identified. Numerical analyses are also carried out to correctly interpret the experimental results. The effectiveness of the proposed control algorithm is compared to that of the classical skyhook algorithm highlighting the validity of the new approach.

2. Modeling of the System's Dynamics

An n-story planar frame structure equipped with an active mass driver system placed on top is considered, as shown in Figure 1. Horizontal displacements of the stories relative to the ground are denoted as $q_1, q_2, \ldots, q_n$, while story masses and stiffness are denoted as $m_1, m_2, \ldots, m_n$ and $k_1, k_2, \ldots, k_n$, respectively.

The AMD system is composed of a ball screw that converts the rotational motion of an electric torsional servomotor into the translational motion of a mass m_a. The total moving mass of the AMD, m_a, is the sum of the mass of the ball nut and the additional carried mass (elements 2 and 6 in Figure 1). The displacement of the movable mass relative to the ground is denoted by q_a, while the rotation of the ball screw is denoted by ϑ. As the motor rotates one revolution, the movable mass is advanced one pitch, l, of the screw. Thus, the following kinematic relation holds for the AMD:

$$\frac{l}{2\pi}\vartheta = q_a - q_n = q_a - \mathbf{F}^T\mathbf{q}, \tag{1}$$

where $\mathbf{q} = [q_1, q_2, \ldots, q_n]^T$ and $\mathbf{F} = [0, 0, \ldots, 1]^T$ are the n-dimensional collocation vector of the AMD.

The servomotor is commanded by assigning an angular velocity to the servodrive of the motor which amplifies such a signal and provides proportional electric current to the motor. An encoder reports the actual status (actual value of the angular velocity measured by the encoder) of the motor to the servodrive, which corrects input current by calculating the deviation between commanded and actual status. Because the device actuation is imperfect, the demand value of the angular velocity ($\dot{\vartheta}_D$) and its actual value ($\dot{\vartheta}_A$) are in general different. This internal dynamics of the actuator can be modeled by accounting for the transfer function between velocity demand value and velocity actual value. However, in the specific problem under consideration, in which the movable mass and the inertia of the screw are small compared to the torque capacity of the servomotor and the command signal is not excessively fast, imperfect actuation of the device is neglected and demand and actual values of the angular velocity are considered coincident.

The free response of the system is governed by the following equation of motion, readily obtained using Lagrange's equations [17]:

$$\begin{aligned} \left(\mathbf{M} + m_a \mathbf{F}\mathbf{F}^T\right)\ddot{\mathbf{q}} + \mathbf{C}\dot{\mathbf{q}} + \mathbf{K}\mathbf{q} &= -\frac{m_a l}{2\pi}\mathbf{F}\ddot{\vartheta} \\ \left(J + \frac{m_a l^2}{4\pi^2}\right)\ddot{\vartheta} &= u_T\left(\dot{\vartheta}\right) - \frac{m_a l}{2\pi}\mathbf{F}\ddot{\mathbf{q}}, \end{aligned} \tag{2}$$

where $\mathbf{M}$, $\mathbf{C}$, and $\mathbf{K}$ are $n \times n$ mass, damping, and system matrices of the frame structure, J is the torsional mass moment of inertia of the ball screw, and $u_T(\dot{\vartheta})$ is the torque provided by the servomotor for the commanded value of the angular velocity.

For active damping of the dynamic response of the substructure it is particularly useful to regulate the inertial force, u, acting on the movable mass. This last is simply given by

$$u = m_a \ddot{q}_a. \tag{3}$$

Substituting (1) into (3) and integrating in time under the assumption of zero initial conditions yield the following equation:

$$\dot{\vartheta} = \frac{2\pi}{m_a l}\int_0^t u(\tau)\,\mathrm{d}\tau - \frac{2\pi}{l}\dot{q}_n, \tag{4}$$

which provides the angular velocity to be commanded to the motor for providing the desired control force u.

3. Nonlinear Control Strategy for Handling Stroke Limits

The movement, x, of real inertial actuators (in the present case $x = q_a - q_n$) is limited by a maximum value, $x_{\max}$, corresponding to the physical stroke extension. Mathematically, such a limitation is represented by a nonholonomic constraint that can be modeled by introducing a proper nonlinear restoring force acting on the movable mass. Such a force can for instance have the following expression, as proposed in [7]:

$$\phi(x) = \left(\frac{x}{x_{\max}}\right)^{2N+1}. \tag{5}$$

Equation (5) corresponds to modeling the impact of the mass against the stroke limit as an elastic (nondissipative) impact, where N is an integer parameter that increases with the increasing rigidity of the physical constraint.

The motion of the inertial mass is in general governed by a feedback control algorithm that accomplishes the task of reducing the vibrations of the substructure. When the relative displacement, x, between the mass and the substructure reaches the value $x_{\max}$, an impact occurs with a consequent exchange of the impulsive force ϕ between the mass and the substructure. This clearly reduces the performance of the control system and can produce damages to the control device as well as to the structural system.

We propose to introduce the stroke limit $x_{\max}$ as a parameter in the control law by coupling a constant gain feedback controller, deputed to dampen structural vibrations, with a nonlinear controller deputed to handle stroke limitation. We denote by u_0 the control signal regulated by the constant gain controller, which is expressed as

$$u_0 = -f(x), \tag{6}$$

where $x = [q, \dot{q}]^T$ is the state vector of the system and f is an appropriate function. This last is, usually, a linear function that can be designed in such a way to guarantee the asymptotic stability of the system and to satisfy some optimal performance criteria. In order to handle the physical limitations imposed on the stroke extension, being impossible to act on $x_{\max}$, it is necessary to gradually stop the actuator when x approaches $x_{\max}$. The easiest way to do it is to introduce in (2) a dissipative force that becomes effective close to the physical limit and is nil elsewhere. Such a force can be obtained with a derivative term with a variable gain given by a constant, G_{NL}, multiplied by a nonlinear x-dependent coefficient $0 \le \varepsilon_{\mathrm{NL}}(x) \le 1$:

$$u = u_0 - G_{\mathrm{NL}}\varepsilon_{\mathrm{NL}}(x)\,\dot{x}. \tag{7}$$

Equation (7) is in the following referred to as "NLC algorithm" where NLC stands for nonlinear control.

The simplest function, $\varepsilon_{\mathrm{NL}}(x)$, to introduce in (7) is a step function that assumes a nil value when $|x|$ is less than $k \cdot x_{\max}$, with $0 \le k \le 1$, and a unit value elsewhere. Unfortunately, this function, which can be expressed as $\varepsilon_{\mathrm{NL}}(x) = H(|x| - k \cdot x_{\max})$ (H denoting the Heaviside step function), is discontinuous for $|x| = k \cdot x_{\max}$ which determines the application of an abrupt brake force requiring a very large electrical power.

In practice the step function is not applicable and does not solve the problem of the abrupt stop of the actuator. In order to solve this problem it is necessary to consider a function, $\varepsilon_{\mathrm{NL}}(x)$, which smoothly varies between 0 and 1 in an interval comprised between $k_0 x_{\max}$ and $k_1 x_{\max}$ with $0 \le k_0 \le k_1 \le 1$. A similar function is here chosen as follows:

$$\varepsilon_{\mathrm{NL}}(x) = \begin{cases} 1, & |x| \geq k_1 x_{\max} \\ 1 - \exp\left(\dfrac{-1}{1 - \left(\left(|x| - k_0 x_{\max} \right) / \left(k_1 x_{\max} - k_0 x_{\max} \right) \right)^2} + 1 \right), & k_0 x_{\max} < |x| < k_1 x_{\max} \\ 0, & |x| \leq k_0 x_{\max}. \end{cases} \tag{8}$$

It is worth noting that $\varepsilon_{\mathrm{NL}}(x)$ given by (8) is an infinitely differentiable function. In particular it does not exhibit any discontinuity and its slope is always finite. This ensures the gradual application of the brake force and the reduction of the associated power. A graphical representation of function $\varepsilon_{\mathrm{NL}}(x)$ is represented in Figure 2(a). It can be shown that $\varepsilon_{\mathrm{NL}}(x)$ tends in norm in the L^2 functional space to the Heaviside function when k_0 and k_1 tend to the same value k. This circumstance is graphically represented in Figure 2(b).

It should be noticed that the linearization of (7) in the origin of the state space, here assumed as a fixed equilibrium point of the system, coincides with the linearization of (6). Therefore, the asymptotic stability of the closed-loop system with control algorithm given by (6) also ensures the local asymptotic stability of the NLC algorithm with $\varepsilon_{\mathrm{NL}}(x)$ given by (8).

A classic skyhook control algorithm is chosen in this work for specializing (6). This strategy results in applying an inertial force to the movable mass that is proportional to the velocity of the top floor relative to the ground and offers the main advantages of being relatively simple to implement and resulting in a significant damping effectiveness.

By regulating u_0 through a skyhook control algorithm, (7) is specialized as follows:

$$u = G_L \dot{q}_n - G_{\mathrm{NL}} \varepsilon_{\mathrm{NL}}(x)\, \dot{x}, \tag{9}$$

where G_L is the constant gain of the skyhook strategy.

The demand value of the angular velocity corresponding to (9) is obtained by substituting such equation into (4) and by time integration under the assumption of zero initial conditions. The following control algorithm is thus obtained where integration by parts of the nonlinear term in (9) has been carried out:

$$\dot{\vartheta} = \frac{2\pi}{l} \left(\frac{G_L q_n}{m_a} - \frac{G_{\mathrm{NL}} \varepsilon_{\mathrm{NL}}(x)\, x}{m_a} + \frac{G_{\mathrm{NL}} \int_0^t \varepsilon'_{\mathrm{NL}} \dot{x} x \, \mathrm{d}\tau}{m_a} - \dot{q}_n \right). \tag{10}$$

In (10), $\varepsilon'_{\mathrm{NL}}$ is the derivative of $\varepsilon_{\mathrm{NL}}$ with respect to x. This quantity is shown in Figure 2(c) and is given by

$$\varepsilon'_{\mathrm{NL}}(x) = \begin{cases} 0, & |x| \geq k_1 x_{\max} \\ \dfrac{2\left(|x| - k_0 x_{\max} \right) \operatorname{sign}(x) \exp\left(\left((-1) \left(1 - \left(\left(|x| - k_0 x_{\max} \right) / \left(k_1 x_{\max} - k_0 x_{\max} \right) \right)^2 \right)^{-1} \right) + 1 \right)}{\left(1 - \left(\left(|x| - k_0 x_{\max} \right) / \left(k_1 x_{\max} - k_0 x_{\max} \right) \right)^2 \right)^2 \left(k_1 x_{\max} - k_0 x_{\max} \right)^2}, & k_0 x_{\max} < |x| < k_1 x_{\max} \\ 0, & |x| \leq k_0 x_{\max}, \end{cases} \tag{11}$$

where $\operatorname{sign}(x)$ is the signum function. It should be noticed that $\varepsilon'_{\mathrm{NL}}(x)$ locally tends to Dirac's delta function for k_0 and k_1 approaching the same value k.

In this work, the integral term appearing in (10) is disregarded under the assumption that it is small compared to the term containing $\varepsilon_{\mathrm{NL}}(x)$. This is true for k_0 which is sufficiently smaller than k_1, that is, for a small value of $\varepsilon'_{\mathrm{NL}}(x)$, also because the product between x and $\dot{x}_n$ is small compared to x. Moreover, $\dot{q}_n$ and q_n in (10) are obtained by online double and single integrations of acceleration signals, respectively.

4. Description of the Experimental Set-Up

The proposed control strategy was tested in the laboratories of the Department of Civil and Environmental Engineering of University of Perugia. A physical model of the structure-AMD system described in Section 2 was designed and constructed. The experimental set-up, shown in Figure 3, is made of the following components: (i) frame structure, (ii) active mass driver, (iii) monitoring sensors, and (iv) controller.

The test structure is a five-story single-bay frame, shown in Figure 3, having a total height of about 1.9 m. The structure is made of steel S 235, whose nominal value of yield strength

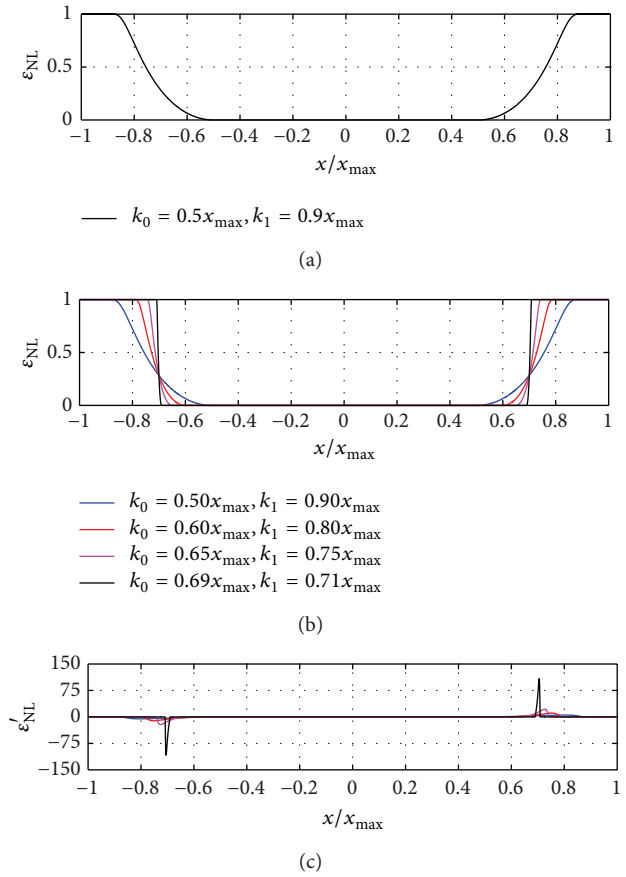

FIGURE 2: Nonlinear function in (8) for a particular choice of parameters k_0 and k_1 (a); nonlinear function in (8) for k_0 and k_1 approaching the same value k (b); derivative of the nonlinear function in (8), expressed by (11), for k_0 and k_1 approaching the same value k (c).

is 235 N/mm^2, according to the Eurocode 3 [18]. Each floor is made of 700 × 300 × 20 mm steel plates of about 32.8 kg weight. The structural configuration consists of the use of 5 × 30 × 340 mm columns for the lowest two stories and 4 × 30 × 340 mm in the remaining ones. The structure is fixed to a support table.

The AMD, installed on the top floor, is composed by a 600 mm long ball screw that converts the rotational motion of a Kollmorgen AKM33H AC servomotor into the translational motion of a 4 kg mass block (approximately 2.5% of the whole structural mass). The maximum speed of the servomotor is 8000 roots per minute and the peak torque is 10.22 Nm. The maximum stroke of the small mass is equal to ±300 mm, while the ball screw has a diameter of 25 mm and a pitch of 25 mm. The whole AMD system, except for its control unit (drive of the servomotor), is mounted on an aluminum plate designed for the purpose that also serves as top floor of the structure.

The position of the mass along the ball screw is measured by means of a JX-P420 linear position transducer. Two optical sensors connected to a logical circuit disable the drive of the motor when the mass exceeds the stroke limits in order to prevent damages of the actuator.

The controller is a National Instruments PXIe-8133 Core i7-820QM, 1.73 GHz, which mounts on board a PXIe-6361 X Series Multifunction DAQ card with 8 channels in differential input. The software installed on the controller is the LabVIEW (LV) real-time. The system fully stands alone and requires the network connection with a host PC only for the initial configuration of the LV code. The communication between the controller and the drive of the motor is based on the EtherCAT protocol.

Six PCB 393C accelerometers are mounted on each floor for the purpose of monitoring structural accelerations. The accelerometers are connected through short cables to the DAQ card by means of the SCB-68 noise rejecting connector block.

5. Experimental and Numerical Tests

Free vibration experimental tests were carried out in order to investigate the effectiveness of the control strategy and to compare experimental results with numerical predictions. Tests were carried out by varying the parameters of the control law to examine their effect on the control effectiveness. The experimental and numerical results were compared to those obtained with the classical skyhook algorithm highlighting the validity of the proposed strategy for handling stroke limitations.

5.1. Free Vibration Tests. To excite the frame structure, the AMD was used as a harmonic shaker located at the top floor of the structure and then, after 10 forcing cycles, the AMD was switched to control. The frequency of excitation was 1.8 Hz, close to the first natural frequency of the frame system.

Two different control strategies were compared: (1) the linear "skyhook" control law (LC); (2) the proposed nonlinear control law (NLC). The corresponding control forces are expressed as

$$\begin{aligned} u &= G_L \dot{q}_n \quad \text{(LC)} \\ u &= G_L \dot{q}_n - G_{NL} \varepsilon_{NL}(x)\, \dot{x} \quad \text{(NLC)}. \end{aligned} \tag{12}$$

The corresponding demand values of the angular velocity are expressed as

$$\dot{\vartheta} = \frac{2\pi}{l}\left(\frac{G_L q_n}{m_a} - \dot{q}_n\right) \quad \text{(LC)} \tag{13}$$

$$\dot{\vartheta} = \frac{2\pi}{l}\left(\frac{G_L q_n}{m_a} - \frac{G_{NL}\varepsilon_{NL}(x)\, x}{m_a} + \frac{G_{NL}\int_0^t \varepsilon'_{NL}\dot{x}x\, d\tau}{m_a} - \dot{q}_n\right) \quad \text{(NLC)}. \tag{14}$$

In Table 1 are summarized the parameters of the control algorithms. The gains G_L and G_{NL} (12) were set equal to 150 and the stroke limit was assumed to be the 90% of the

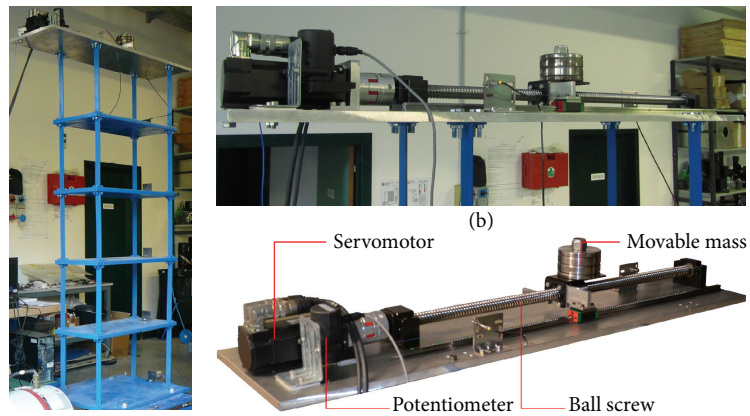

Figure 3: Experimental set-up: overview of the system (a); detailed views of the AMD (b-c).

Table 1: Performance indices of the control effectiveness computed adopting the experimental results.

Parameter	Value
G_L	150
G_{NL}	150
$x_{\max}$	6.8 cm
k_1	0.8
k_0	0.2–0.7

maximum stroke of the movable mass obtained with the LC strategy. The coefficient k_1 was selected as 0.8 and k_0 was varied between 0.2 and 0.7.

Figure 4 shows the top floor displacements of the uncontrolled and controlled system with LC and NLC strategies. During the loading phase the structural displacements increase while, when the control is switched on, the structural response is rapidly decreased by both of the adopted control approaches.

Figure 5 shows the results in terms of AMD displacements and top floor displacements obtained with the LC and the NLC algorithms for $k_0 = 0.2$ and $k_1 = 0.8$. It is also shown for comparison with the nonlinear velocity demand that is activated when the AMD stroke exceeds the value $k_0\, x_{\max}$. Neglecting the integral term in (14), the nonlinear velocity demand is the difference between the total velocity demands expressed by (14) and (13) and is written as

$$\dot{\vartheta}_{\mathrm{NL}} = \frac{2\pi}{l}\frac{G_{\mathrm{NL}}\varepsilon_{\mathrm{NL}}(x)\,x}{m_a}. \tag{15}$$

It is possible to observe that, adopting the NLC strategy, the AMD stroke never exceeds $x_{\max}$. Although the control algorithm is not recentering, the nonlinear algorithm contributes to limiting the residual AMD displacement, thus avoiding the need for manual or automatic recentering after the seismic event. The small residual displacement regards the AMD only while the substructure elastically recovers its initial configuration after the vibration is dissipated. The

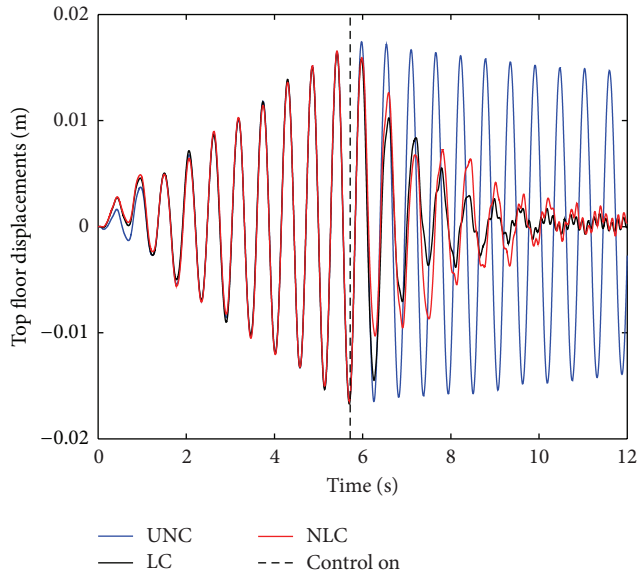

Figure 4: Top floor displacements for the uncontrolled (UNC) and controlled systems with LC and NLC ($k_0 = 0.2$) strategies.

difference between the structural response obtained with LC and NLC algorithms appears after the first peak of the controlled response when the AMD stroke has exceeded the value $k_0 x_{\max}$ and the nonlinear restoring force is activated. As expected, after the second peak the control performance obtained with the NLC algorithm is slightly worse than that obtained with the LC law. However, the damping provided to the structure is sufficient to rapidly decrease the structural response in both cases (Figure 4).

Figure 6 shows the velocity demand obtained with both the classic skyhook (LC) and the proposed nonlinear control (NLC) strategies (13)-(14). The difference of the two lines in Figure 6 represents the nonlinear velocity demand plotted at the bottom of Figure 5. A peak of the AMD velocity in correspondence of the first braking of the movable mass is visible. After the first peak, the velocity demand required by the two algorithms is almost comparable.

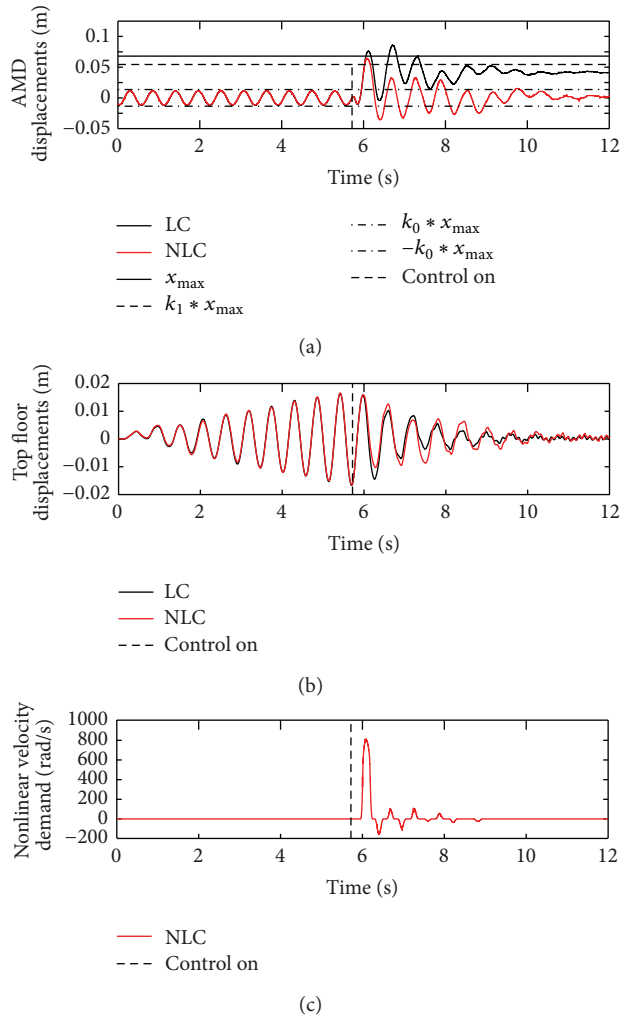

FIGURE 5: AMD displacements (a); top floor displacements (b); nonlinear velocity demand expressed by (15) (c) for the controlled system.

In practical applications, control force saturation can likely occur as the nonlinear control system requires a significant power demand to produce the first braking of the AMD. To study the effect of force saturation, additional tests were carried out. In particular, by properly setting the controller, the actual velocity supplied by the servomotor was limited to 150 rad/s, value well below the physical limit of the system. Figure 7 shows that the proposed control algorithm is effective in reducing the structural response and avoiding the stroke limits crossing even in presence of such force saturation.

To quantify the effectiveness of the control strategy, the following performance indices are defined:

$$J_1 = \frac{\max_{t>t_0} |q_a - q_5|^{\mathrm{NLC}}}{\max_{t>t_0} |q_a - q_5|^{\mathrm{LC}}},$$

$$J_2 = \frac{\max_{t>t_0,i} \left|q_i^{\mathrm{NLC}}\right|}{\max_{t>t_0,i} \left|q_i^{\mathrm{LC}}\right|},$$

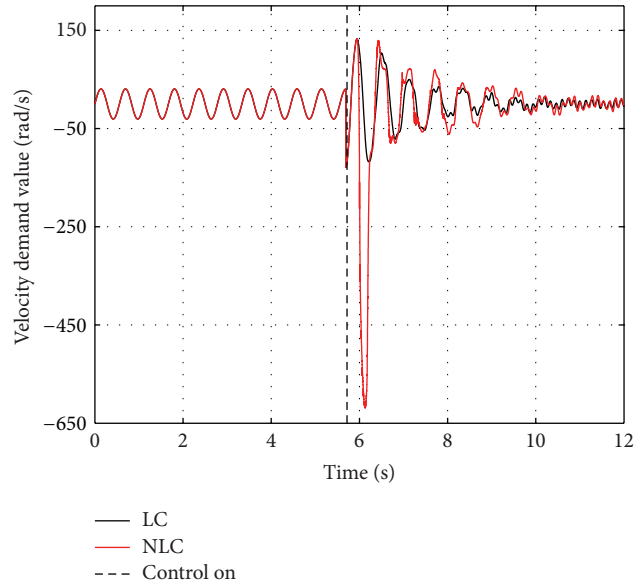

FIGURE 6: Velocity demand obtained with LC and NLC ($k_0 = 0.2$) strategies.

TABLE 2: Performance indices of the control effectiveness computed adopting the experimental results.

k_0	J_1	J_2	J_3	J_4	J_5
0.2	0.749	0.987	1.102	0.995	4.642
0.3	0.767	1.001	1.077	1.004	4.803
0.4	0.843	1.012	1.010	1.208	5.117
0.5	0.857	1.008	1.139	1.268	5.332
0.6	0.862	1.005	0.947	1.214	5.541
0.7	0.891	1.059	1.109	1.226	5.603

$$J_3 = \frac{\mathrm{rms}_{t>t_0,i} \left|q_i^{\mathrm{NLC}}\right|}{\mathrm{rms}_{t>t_0,i} \left|q_i^{\mathrm{LC}}\right|},$$

$$J_4 = \frac{\max_{t>t_0,i} \left|\ddot{q}_i^{\mathrm{NLC}}\right|}{\max_{t>t_0,i} \left|\ddot{q}_i^{\mathrm{LC}}\right|},$$

$$J_5 = \frac{\max_{t>t_0} \left|\dot{\vartheta}_D^{\mathrm{NLC}}\right|}{\max_{t>t_0} \left|\dot{\vartheta}_D^{\mathrm{LC}}\right|}, \tag{16}$$

where J_1 is the ratio of the maximum relative displacements between the AMD (q_a) and the top floor (q_5) obtained with the NLC and the LC strategies; J_2 is the ratio of the maximum floor displacements (q_i) obtained with the NLC and the LC strategies; J_3 is the ratio of the root mean square of the floor displacements obtained with the NLC and the LC strategies; J_4 is the ratio of the maximum floor accelerations ($\ddot{q}_i$) obtained with the NLC and the LC strategies; J_5 is the ratio of the maximum velocity demand value ($\dot{\vartheta}_D$) obtained with the NLC and the LC strategies.

In Table 2 are shown the performance indices corresponding to experimental responses obtained for different

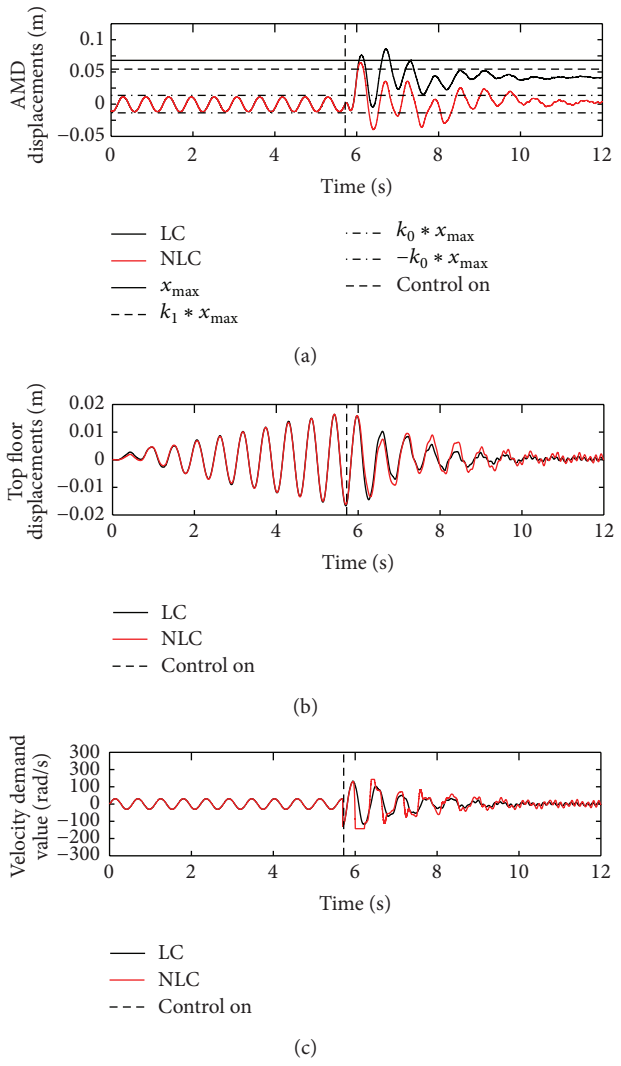

Figure 7: AMD displacements (a); top floor displacements (b); nonlinear velocity demand (c); for the system controlled with LC and NLC algorithms ($k_0 = 0.2$) in case of force saturation.

values of parameter k_0. The value $k_0 = 0.8$ was not considered because, as observed in Section 3, when $k_0 = k_1$, $\varepsilon_{NL}(x)$ essentially coincides with Heaviside's step function which cannot be reproduced in practice.

The results in Table 2 show that if k_0 increases, (i) the braking efficacy decreases (as J_1 increases), (ii) the control performance is slightly worsened (as J_2 increases), (iii) the ratio of the root mean square of the top displacements obtained with the NLC and the LC (J_3) is generally higher than one, (iv) the structural acceleration induced by the braking term increases (as J_4 increases), and (v) due to the additional nonlinear term, the velocity demand increases with respect to the LC case (as J_5 increases).

Based on the obtained results it can be concluded that the NLC is effective in reducing the structural response and avoiding the stroke limit crossing, at the expense of an almost negligible increase in structural displacements and a slight increase in structural accelerations. For free response vibrations, the increase in power demand with respect to the LC case is important only for the first braking peak and the possible force saturation does not significantly deteriorate the control performance.

Table 3: Identified modal characteristics of the system.

Mode	Natural frequency (Hz)	Modal damping ratio (%)
1	1.76	0.3
2	4.92	0.4
3	7.34	1.1
4	9.62	1.2
5	12.15	1.3

Table 4: Performance indices of the control effectiveness computed adopting the numerical results.

k_0	J_1	J_2	J_3	J_4	J_6
0.2	0.585	1.000	1.000	1.000	1.943
0.3	0.619	1.000	1.000	1.000	2.412
0.4	0.651	1.000	1.000	1.000	2.392
0.5	0.681	1.000	1.000	1.000	2.737
0.6	0.711	1.000	1.000	1.000	3.268
0.7	0.740	1.000	1.000	1.000	4.097

5.2. Numerical Simulations and Discussion. Numerical analyses were performed to better interpret the experimental results and further discuss the effectiveness of the control strategy.

Preliminarily, a numerical model was built and tuned to the free vibration response of the uncontrolled system. A modal identification allowed obtaining an accurate numerical model of the system, considered as a shear-type structure having 5 degrees of freedom. The signals provided by the 5 accelerometers located on the floors, recorded with a sampling frequency of 1 kHz and a total duration of 1 hour, were used for modal identification. The structural response signals were acquired with excitation provided by microtremors in the laboratory. The Frequency domain decomposition (FDD) was used to perform the modal identification after decimation of the measured time history signals to 50 Hz and using a frequency resolution to compute the power spectral density matrix of the measurements equal to 0.0122 Hz. The results of modal identification are summarized in Table 3. After identifying the dynamic characteristics of the physical system, a model tuning was performed to obtain the masses and stiffness coefficients of the frame to be adopted in the numerical model, as detailed in [17]. In Table 3 are also reported the modal damping ratios obtained by analyzing the envelopes of the free decay responses of the five structural modes. Single mode responses are obtained by harmonically exciting the structure with the AMD working as a shaker providing excitation in resonance with a specific mode. Considering that the modal damping ratios vary slightly with the amplitude of vibration, their values are estimated in intermediate ranges of the response.

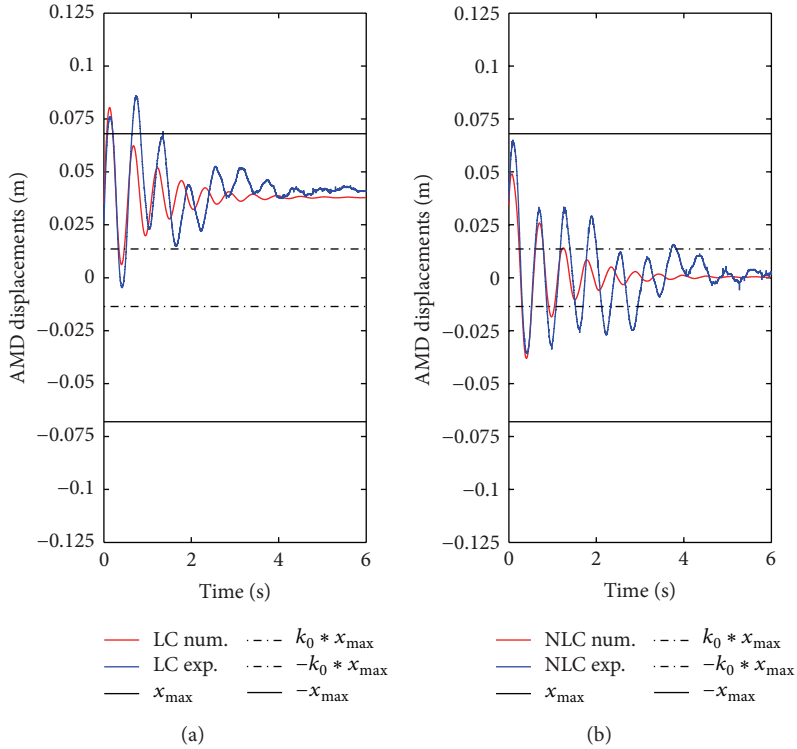

FIGURE 8: Comparison between numerical and experimental AMD displacements for LC (a) and NLC (b).

The experimental tests were reproduced numerically applying at the top of the structure a sinusoidal inertial force corresponding to the acceleration of the AMD. Figure 8 shows the comparison between numerical and experimental AMD displacements for both LC ($G_L = 150$) and NLC strategies ($G_{NL} = 150, k_0 = 0.2, k_1 = 0.8$). The comparison is limited to the controlled part of the response. The experimental and numerical results are close to each other, especially for the first and second peaks of the response. Nevertheless, there are still some deviations in the rate of decay and the phase of the response due to the imperfect actuation of the AMD.

Similar observations can be drawn for Figure 9, representing the comparison between the numerical and experimental top floor displacements. Although there is a relatively good correspondence between the experimental and numerical results obtained at the beginning of the control phase, the experimental response decay appears different due to the internal dynamics of the actuator.

Figure 10 reports the comparison between the numerically predicted control force obtained with LC and NLC strategies. The NLC algorithm leads to an important increase in the control force at the beginning of the actuation.

In Table 4 are summarized the performance indices, introduced in Section 5.1, computed by adopting the numerical results. The index J_5 is computed by using the control force instead of the velocity demand value as follows:

$$J_6 = \frac{\max_{t>t_0} \left|u^{\mathrm{NLC}}\right|}{\max_{t>t_0} \left|u^{\mathrm{LC}}\right|}, \tag{17}$$

where u is given by (12). It is clear from the results that, being equal to the gain G_{NL}, the braking performance is reduced with the increase of the coefficient k_0. The indices J_2, J_3, and J_4 are equal to 1 for all the analyzed cases, meaning that, at the first peak, the LC and NLC algorithms provide the same structural response. The index J_5 suggests that the difference between the control force yielded by NLC and LC strategies increases as k_0 increases. The discrepancy between the results reported in Tables 2 and 4 can be ascribed to the imperfect experimental actuation and the small differences between the physical and numerical models.

6. Conclusions

In this paper, a nonlinear control strategy based on a modified direct velocity feedback algorithm is proposed for handling stroke limits of an AMD system. In particular, a nonlinear braking term proportional to the relative AMD velocity is included in the control algorithm in order to slowdown the device in the proximity of the stroke limits.

Experimental and numerical tests were carried out on a scaled-down five-story building equipped with an AMD under free vibrations.

The proposed nonlinear control law proved to be effective in reducing the structural response and avoiding the stroke limit crossing, at the expense of a small increase of structural displacements and a slight increase of structural accelerations. The growth in power demand with respect to the linear case is important only for the first braking peak and the possible force saturation does not interfere significantly with

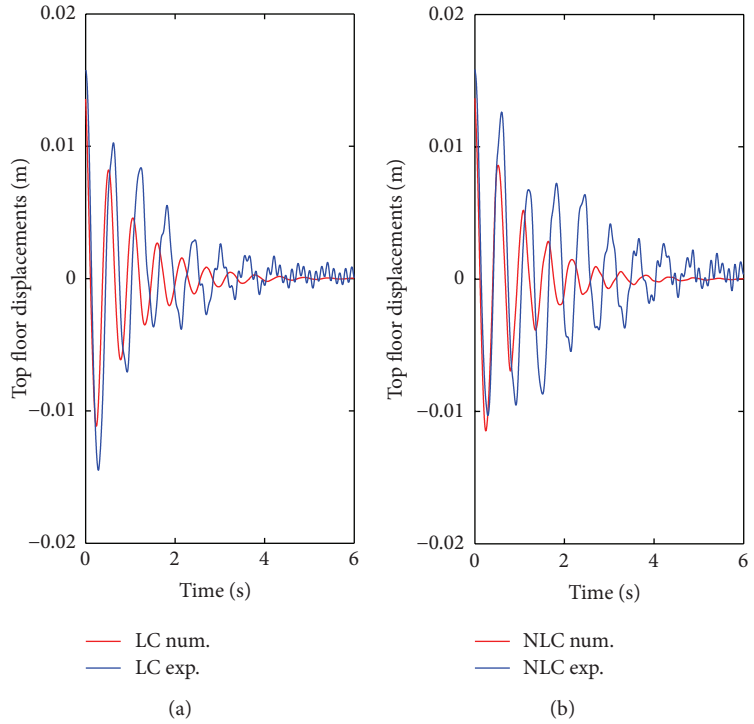

Figure 9: Comparison between numerical and experimental top displacements for LC (a) and NLC (b).

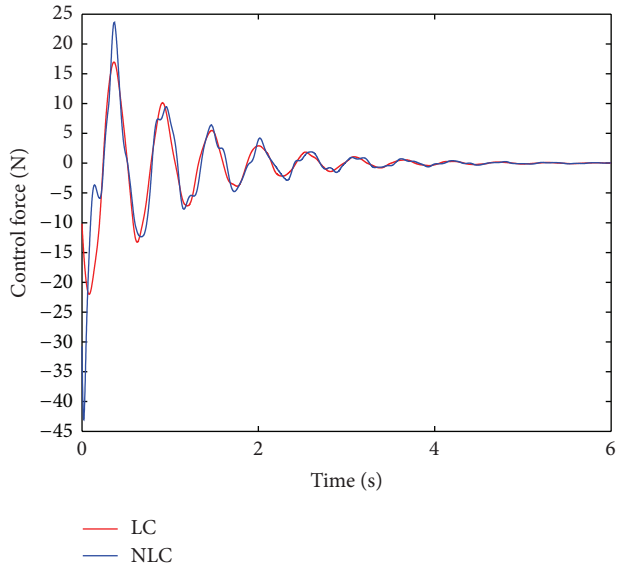

Figure 10: Control force obtained with the numerical analyses.

the control performance. The parametric analysis showed that an increase of the ratio k_1/k_0 between the parameters defining the nonlinear restoring force results in an improved performance in terms of braking efficacy. On the contrary, the same braking efficacy can be obtained with a lower k_1/k_0 ratio and a higher gain G_{NL}, at the expense of an increase in the structural response, especially in terms of accelerations. The optimal choice of the ratio k_1/k_0 should be obtained as a compromise between the need of limiting the power demand and that of limiting the structural response.

Conflict of Interests

The authors declare that there is no conflict of interests regarding the publication of this paper.

Acknowledgments

The authors gratefully acknowledge the financial support of the "Cassa di Risparmio di Perugia" Foundation that funded this study through the project "Development of active control systems for the response mitigation under seismic excitation" (Project no. 2010.011.0490). Suggestions and comments by Dr. Michele Moretti and Dr. Matteo Becchetti, University of Perugia, are also acknowledged with gratitude.

References

[1] I. Venanzi and A. L. Materazzi, "Acrosswind aeroelastic response of square tall buildings: a semi-analytical approach based of wind tunnel tests on rigid models," *Wind & Structures*, vol. 15, no. 6, pp. 495–508, 2012.

[2] I. Venanzi and A. L. Materazzi, "Multi-objective optimization of wind-excited structures," *Engineering Structures*, vol. 29, no. 6, pp. 983–990, 2007.

[3] A. Forrai, S. Hashimoto, H. Funato, and K. Kamiyama, "Robust active vibration suppression control with constraint on the control signal: application to flexible structures," *Earthquake*

Engineering & Structural Dynamics, vol. 32, no. 11, pp. 1655–1676, 2003.

[4] J. G. Chase, S. E. Breneman, and H. A. Smith, "Robust H_∞ static output feedback control with actuator saturation," *Journal of Engineering Mechanics*, vol. 125, no. 2, pp. 225–233, 1999.

[5] B. Indrawan, T. Kobori, M. Sakamoto, N. Koshika, and S. Ohrui, "Experimental verification of bounded-force control method," *Earthquake Engineering & Structural Dynamics*, vol. 25, no. 2, pp. 179–193, 1996.

[6] J. R. Cloutier, "State-dependent Riccati equation techniques: an overview," in *Proceedings of the American Control Conference*, pp. 932–936, Albuquerque, NM, USA, 1997.

[7] B. Friedland, "On controlling systems with state-variable constraints," in *Proceedings of the American Control Conference*, pp. 2123–2127, Philadelphia, Pa, USA, 1998.

[8] A. L. Materazzi and F. Ubertini, "Robust structural control with system constraints," *Structural Control and Health Monitoring*, vol. 19, no. 3, pp. 472–490, 2012.

[9] J.-H. Kim and F. Jabbari, "Actuator saturation and control design for buildings under seismic excitation," *Journal of Engineering Mechanics*, vol. 128, no. 4, pp. 403–412, 2002.

[10] J. Mongkol, B. K. Bhartia, and Y. Fujino, "On Linear-Saturation (LS) control of buildings," *Earthquake Engineering & Structural Dynamics*, vol. 25, no. 12, pp. 1353–1371, 1996.

[11] Z. Wu and T. T. Soong, "Modified bang-bang control law for structural control implementation," *Journal of Engineering Mechanics*, vol. 122, no. 8, pp. 771–777, 1996.

[12] C.-W. Lim, "Active vibration control of the linear structure with an active mass damper applying robust saturation controller," *Mechatronics*, vol. 18, no. 8, pp. 391–399, 2008.

[13] I. Nagashima and Y. Shinozaki, "Variable gain feedback control technique of active mass damper and its application to hybrid structural control," *Earthquake Engineering & Structural Dynamics*, vol. 26, no. 8, pp. 815–838, 1997.

[14] M. Yamamoto and T. Sone, "Behavior of active mass damper (AMD) installed in high-rise building during 2011 earthquake off Pacific coast of Tohoku and verification of regenerating system of AMD based on monitoring," *Structural Control and Health Monitoring*, vol. 21, no. 4, pp. 634–647, 2013.

[15] I. Venanzi, F. Ubertini, and A. L. Materazzi, "Optimal design of an array of active tuned mass dampers for wind-exposed high-rise buildings," *Structural Control and Health Monitoring*, vol. 20, pp. 903–917, 2013.

[16] I. Venanzi and A. L. Materazzi, "Robust optimization of a hybrid control system for wind-exposed tall buildings with uncertain mass distribution," *Smart Structures and Systems*, vol. 12, no. 6, pp. 641–659, 2013.

[17] F. Ubertini, I. Venanzi, G. Comanducci, and A. L. Materazzi, "On the control performance of an active mass driver system," in *Proceedings of the AIMETA Congress*, Turin, Italy, 2013.

[18] EN 1993-1-1 Eurocode 3: Design of steel structures—part 1-1: General rules and rules for buildings, 2005.